Advanced Mathematical Modeling of Sonar-Induced Bubble Growth and Coalescence in Humans and Marine Mammals

September 2008

by

Yurii A. Ilinskii, Preston S. Wilson, and Mark F. Hamilton

Applied Research Laboratories
\The University of Texas at Austin
P.O. Box 8029
Austin, Texas 78713-8029

20081001439

REPORT DOCUMENTATION PAGE

1. REPORT DATE *(DD-MM-YYYY)*	2. REPORT TYPE	3. DATES COVERED *(From - To)*
09-29-2008	Final	FEB 2005 – JULY 2008

4. TITLE AND SUBTITLE

Advanced Mathematical Modeling of Sonar-Induced Bubble Growth and Coalescence in Humans and Marine Mammals—Final Report to the Office of Naval Research Under the Support of Grant N00014-05-1-0292

5a. CONTRACT NUMBER

5b. GRANT NUMBER
N00014-05-1-0292

5c. PROGRAM ELEMENT NUMBER

6. AUTHOR(S)
Ilinskii, Yurii A.
Wilson, Preston S.
Hamilton, Mark F.

5d. PROJECT NUMBER

5e. TASK NUMBER

5f. WORK UNIT NUMBER

7. PERFORMING ORGANIZATION NAME(S) AND ADDRESS(ES)

Applied Research Laboratories
The University of Texas at Austin
P.O. Box 8029
Austin, TX 78713-8029

8. PERFORMING ORGANIZATION REPORT NUMBER

9. SPONSORING/MONITORING AGENCY NAME(S) AND ADDRESS(ES)

Office of Naval Research
875 North Randolph Street
Arlington, VA 22203-1995

10. SPONSOR/MONITOR'S ACRONYM(S)
ONR

11. SPONSOR/MONITOR'S REPORT NUMBER(S)

12. DISTRIBUTION/AVAILABILITY STATEMENT
Approved for Public Release; distribution is Unlimited

13. SUPPLEMENTARY NOTES

14. ABSTRACT

For high gas supersaturation levels in liquids, on the order of 300% as predicted in capillaries of marine mammals following a series of dives, standard mathematical models of both static and rectified diffusion are found to underestimate the rate of bubble growth by 10%–20%. The discrepancy is demonstrated by comparing predictions based on existing mathematical models with direct numerical solutions of the differential equations for gas diffusion in the liquid and thermal conditions in the bubble. Underestimation of bubble growth by existing mathematical models is due to the underlying assumption that the gas concentration in the liquid is given by its value for a bubble of constant equilibrium radius. This assumption is violated when high supersaturation causes the bubble to grow too fast in relation to the time scale associated with diffusion. Rapid bubble growth results in an increased gas concentration gradient at the bubble wall, and therefore a growth rate in excess of predictions based on constant equilibrium bubble radius. The effect of gas supersaturation level, excitation frequency, duty cycle and sound pressure level on bubble growth were also studied.

15. SUBJECT TERMS
bubble growth, rectified diffusion, marine mammals, sonar

16. SECURITY CLASSIFICATION OF:			17. LIMITATION OF ABSTRACT	18. NUMBER OF PAGES	19a. NAME OF RESPONSIBLE PERSON
a. REPORT	b. ABSTRACT	c. THIS PAGE			Preston S. Wilson
U	U	U	UU	30	19b. TELEPHONE NUMBER *(Include area code)* 512-475-9093

Advanced Mathematical Modeling of Sonar-Induced Bubble Growth and Coalescence in Humans and Marine Mammals—Final Report to the Office of Naval Research Under the Support of Grant N00014-05-1-0292

Yurii A. Ilinskii, Preston S. Wilson, and Mark F. Hamilton

Applied Research Laboratories, The University of Texas at Austin, Austin, Texas 78713-8029

Abstract

For high gas supersaturation levels in liquids, on the order of 300% as predicted in capillaries of marine mammals following a series of dives [Houser et al., J. Theor. Biol. **213**, 183–195 (2001)], standard mathematical models of both static and rectified diffusion are found to underestimate the rate of bubble growth by 10%–20%. The discrepancy is demonstrated by comparing predictions based on existing mathematical models with direct numerical solutions of the differential equations for gas diffusion in the liquid and thermal conditions in the bubble. Underestimation of bubble growth by existing mathematical models is due to the underlying assumption that the gas concentration in the liquid is given by its value for a bubble of constant equilibrium radius. This assumption is violated when high supersaturation causes the bubble to grow too fast in relation to the time scale associated with diffusion. Rapid bubble growth results in an increased gas concentration gradient at the bubble wall, and therefore a growth rate in excess of predictions based on constant equilibrium bubble radius. The effect of gas supersaturation level, excitation frequency, duty cycle and sound pressure level on bubble growth were also studied.

I. INTRODUCTION

There is continued interest in possible effects of underwater sound on the growth of gas bubbles in capillaries of marine mammals and humans. Numerical simulations motivated by this interest have been reported by Crum and Mao, [1] who considered gas supersaturation levels up to 223%. Houser et al. [2] subsequently calculated the evolution of the nitrogen tension and relative supersaturation due to typical diving profiles executed by dolphins, blue whales and beaked whales. Supersaturation levels were predicted to reach 250%–300% upon completion of the dive profiles, depending upon the species. The highest level of 300% was predicted for beaked whales.

One assumption in existing models is that supersaturation in the liquid far from the bubble is constant. However, for constant external pressure P_0 the gas concentration C decays to its equilibrium level C_0 according to the kinetic equation

$$\frac{dC}{dt} = -\frac{C - C_0}{t_w},\qquad(1)$$

where $t_w = t_h/\ln 2$ is the exponential time constant for nitrogen washout, and t_h is the corresponding half-time. Ridgway and Howard [3] measured $t_h \sim 6$ min for washout from dolphin muscle tissue. Other assumptions underlying existing models include large Péclet numbers (dimensionless ratio of frequency to diffusion coefficient), coefficients that do not depend on pressure and temperature, linear theory for thermal and radiation damping of the bubble oscillations, and gas concentration in the liquid given by its value for a bubble of constant equilibrium radius. All of these assumptions can be analyzed numerically. The purpose of our paper is to present a relatively efficient numerical scheme for performing such calculations and to compare results with those from previous work. It is found that the last approximation, that of neglecting the effect of the rate at which the equilibrium bubble radius grows on the gas concentration in the surrounding liquid, leads to underestimation of bubble growth rate by 10%–20% at high supersaturation levels.

While recent work on bubble growth in marine mammals at high gas supersaturation levels motivated the present study, it is not the purpose of this paper to speculate on the impact of our study in this context. *In vivo* bubble dynamics is a complicated process affected by many factors, such as constraints imposed by tissue, nonspherical bubble shapes, and surfactants. Also to be considered is the matter of nucleation. [4] Uncertainties associated with such additional factors can easily dominate the contribution due to the percentage

2

change in growth rate predicted here in connection with rectified diffusion in an unbounded liquid. We nevertheless performed our calculations for sound pressure levels that may be of interest in studies of the effects of underwater sound on marine mammals, for which the percentage change in equilibrium radius predicted by the model presented here is at most about 20%.

In Sections II and III, a new model for bubble growth by static and rectified diffusion, applicable to high gas concentration levels, is developed and then compared to the predictions of existing models in Section IV. The effect on bubble growth of a range of sonar parameters, including frequency, amplitude, duty cycle, repetition rate, and ping type is also presented in Section IV. Conclusions are presented in Section V.

II. THEORETICAL MODELS

A. Static (nonacoustic) diffusion

The basis for all existing theoretical models is Epstein and Plesset's model [5] for static (nonacoustic) diffusion. The diffusion equation for spherical symmetry is

$$\frac{\partial C}{\partial t} = \frac{D}{r^2} \frac{\partial}{\partial r} \left(r^2 \frac{\partial C}{\partial r} \right), \tag{2}$$

where D is the diffusion constant. The initial concentration of the gas at $t = 0$ is assumed to be uniform and given by C_∞, and for $t > 0$ the gas concentration C_R at the bubble wall is determined by Henry's law,

$$C_R = P_g / H_D, \tag{3}$$

where P_g is gas pressure in the bubble, and H_D is Henry's constant. The equilibrium concentration of gas in a liquid at a planar boundary and for a given pressure P_0 in the liquid is $C_0 = P_0 / H_D$. At the surface of a spherical gas bubble we have, when vapor pressure is negligible,

$$\frac{C_R}{C_0} = 1 + \frac{2\sigma}{P_0 R_0}, \tag{4}$$

where R_0 is the bubble radius and σ is the surface tension, which are related through $P_g = P_0 + 2\sigma / R_0$.

Epstein and Plesset [5] used the above relations to derive the following result for the rate

3

of change in bubble radius:

$$\frac{dR_0}{dt} = \frac{Dd}{1 + 4\sigma/3P_0R_0}\left[\frac{C_\infty}{C_0} - \left(1 + \frac{2\sigma}{P_0R_0}\right)\right] \times \left(\frac{1}{R_0} + \frac{1}{\sqrt{\pi Dt}}\right),$$ (5)

where $d = k_BT/H_D$ is a dimensionless parameter, T is temperature, and k_B is Boltzmann's constant. The physical sense of this parameter is that, for a given temperature, it is the ratio of dissolved gas concentration near the bubble wall, C_R, to the density of gas in the bubble. According to Henry's law, Eq. (3), this ratio does not depend on concentration. However, it does depend on temperature.

It follows from Eq. (5) that the bubble loses mass $(dR_0/dt < 0)$ for $C_\infty < C_R$. When the liquid far from the bubble is saturated $(C_\infty = C_0)$ Eq. (4) yields $C_R > C_\infty$, and the bubble dissolves. Only for $C_\infty = C_R = C_0(1 + 2\sigma/P_0R_0)$, i.e., for which the supersaturation is given by $1 + 2\sigma/P_0R_0$, is the bubble stabilized. For supersaturation greater than this value the bubble will grow.

When effects of surface tension are ignored $(\sigma = 0)$, and for bubble radius sufficiently large $(R_0 \gg 2\sigma/P_0)$, Eq. (5) can be solved analytically. [5] However, the analytical solution for this case exists only in complicated parametric form and can be analyzed only by plotting graphs for different parameters. In this case it is preferable to solve Eq. (5) numerically.

Equation (5) is derived from the gas mass flow estimated using the diffusion equation with the boundary condition imposed on a bubble of constant radius. This approach is valid only for low levels of supersaturation and when the bubble growth rate is sufficiently small. Also, the initial conditions are constant gas concentration everywhere from infinity to the bubble wall. Therefore at the initial time $t = 0$ there is a jump in the gas concentration across the bubble wall. The gradient across this jump in gas concentration is thus singular at $t = 0$, and it is the source of the singular term $1/\sqrt{\pi Dt}$ that appears in Eq. (5). The nonsingular term that contains $1/R_0$ corresponds to the gradient of the concentration at the bubble wall for the stationary concentration

$$C(r) = C_\infty + (C_R - C_\infty)\frac{R_0}{r}.$$ (6)

For initial conditions that correspond to this stationary concentration there is no singularity. Therefore, results depend on the initial concentration, and a stationary initial concentration is more realistic than one that is singular.

4

B. Gas diffusion outside bubble with changing radius

Fick's law, Eq. (2) with a convection term included, is used to account for motion of the bubble wall. Using a transformed version of Fick's law in Lagrangian coordinates, Eller and Flynn [6, 7] have shown that for the case of a small dimensionless parameter $1/\mathrm{Pe} = D/\omega R_0^2$, or large Péclet number Pe, where ω is a characteristic angular frequency of the bubble motion, the equation for the equilibrium bubble radius becomes

$$
\frac{dR_0}{dt} = \frac{Dd}{1 + 4\sigma/3P_0R_0} \left(\frac{C_\infty}{C_0} - \frac{\langle P_g R^4 \rangle}{P_0 \langle R^4 \rangle} \right) \\
\times \left[\frac{\langle R \rangle}{R_0^2} + \left(\frac{\langle R^4 \rangle}{R_0^4 \pi Dt} \right)^{1/2} \right],
\tag{7}
$$

where $R(t)$ is the instantaneous bubble radius, and the angular brackets indicate time averaging.

Fyrillas and Szeri [8] subsequently improved Eq. (7) by splitting the transformed Fick's equation into an equation for the rapidly oscillating part of the solution and another equation for the slowly varying part, for the same asymptotic case of large Péclet number. They showed that the solution of the oscillatory problem yields zero mean flux of gas particles through the bubble wall. To solve the problem for the slowly varying part they used a standard averaging method to obtain

$$
\frac{dR_0}{dt} = \frac{Dd}{1 + 4\sigma/3P_0R_0} \left(\frac{C_\infty}{C_0} - \frac{\langle P_g R^4 \rangle}{P_0 \langle R^4 \rangle} \right) \\
\times \frac{1}{R_0} \int_0^\infty \frac{dx}{\langle [3x + (R/R_0)^3]^{4/3} \rangle}.
\tag{8}
$$

The singularity $1/\sqrt{\pi Dt}$ was not retained in this formulation.

Both Eqs. (7) and (8) were used by Crum and Mao [1] in their numerical simulations. In general the time averages in these equations must be calculated using numerical solutions of the Rayleigh-Plesset equation. Crum and Mao also discuss an analytical approximation of these time averages, valid only for small bubble oscillations, based on a perturbation solution of the Rayleigh-Plesset equation in powers of the small parameter P_a/P_0, where P_a is the acoustic pressure.

III. NUMERICAL MODEL

The starting point for our numerical model is the form of the diffusion equation, Fick's equation in Lagrangian spherical coordinates, obtained by Eller and Flynn [7] and used by Fyrillas and Szeri: [8]

$$\frac{\partial C}{\partial t} = D \frac{\partial}{\partial s} \left[(3s + R^3)^{4/3} \frac{\partial C}{\partial s} \right],$$ (9)

where $3s = r^3 - R^3 = r_L^3 - R_0^3$, and where r_L is the Lagrangian radial coordinate, and r is the Eulerian radial coordinate. The bubble radius R obeys an ordinary differential equation. We will use a standard form of the Rayleigh-Plesset equation,

$$R\ddot{R} + \frac{3}{2}\dot{R}^2 = \frac{1}{\rho} \left(P_g - P_0 - P_a \cos \omega t - \frac{2\sigma}{R} - 4\mu \frac{\dot{R}}{R} \right),$$ (10)

where ρ is the density of the liquid, σ is the surface tension, μ is viscosity, P_a and ω are the amplitude and frequency of the acoustic field in the vicinity of the bubble, respectively, P_0 is the ambient pressure, and P_g is the pressure of the gas in the bubble. In absence of an acoustic field $P_g = P_{g0} = P_0 + 2\sigma/R_0$. The number N of gas molecules in the bubble obeys the equation

$$\frac{dN}{dt} = 4\pi R^2 D \frac{\partial C}{\partial r},$$ (11)

where the derivative $\partial C/\partial r$ is calculated at the bubble wall, $r = R$.

The boundary conditions on the bubble wall and at infinity are, respectively,

$$C(s = 0) = C(r_L = R_0) = C_R = \frac{P_g}{H_D},$$ (12)

$$C(s = \infty) = C(r_L = \infty) = C_\infty.$$ (13)

To avoid the boundary condition at infinity, or for very large r_L, we transform Eq. (9) using the dimensionless, reciprocal distance $\xi = R_0/r_L$:

$$\frac{\partial C}{\partial t} = \frac{D}{R_0^2} \xi^4 \frac{\partial}{\partial \xi} \left\{ \left[1 + \xi^3 \left(\frac{R^3}{R_0^3} - 1 \right) \right]^{4/3} \frac{\partial C}{\partial \xi} \right\},$$ (14)

where $\xi \in (0, 1)$. The boundary conditions for Eq. (14) are

$$C(\xi = 1) = C_R, \qquad C(\xi = 0) = C_\infty,$$ (15)

and Eq. (11) becomes

$$\frac{dN}{dt} = -\frac{4\pi D R^4}{R_0^3} \frac{\partial C}{\partial \xi},$$ (16)

6

where the derivative $\partial C / \partial \xi$ is calculated at $\xi = 1$.

An implicit finite difference scheme with a homogeneous grid on the interval $\xi \in (0, 1)$ was developed to solve Eq. (14). The coordinate ξ is particularly convenient for these calculations because it provides a dense grid in real space near the bubble wall, where the gradient of the concentration is greatest.

A.   Radiation losses

The influence of liquid compressibility on the dynamics of a single bubble has been discussed in many papers. [9–11] In Ref. [12] it was shown that the influence of compressibility can be taken into account by adding the term $\dddot{V}/4\pi c$ to the right-hand side of Eq. (10), where V is the bubble volume, and c is the sound speed in the liquid. When expanded in terms of the bubble radius this correction term becomes $(R^2 \dddot{R} + 6R\dot{R}\ddot{R} + 2\dot{R}^3)/c$, which coincides with the terms obtained previously by Prosperetti [10] to account for compressibility. In particular, it accounts for additional energy loss during bubble oscillations through acoustic radiation.

We now rewrite $\dddot{V}/4\pi c$ as follows:

$$\frac{\dddot{V}}{4\pi c} = \frac{1}{3c} \frac{d^3 R^3}{dt^3} = \frac{1}{c} \frac{d}{dt} [R(R\ddot{R} + 2\dot{R}^2)] . \tag{17}$$

Making use of the fact that the correction to the Rayleigh-Plesset equation that accounts for compressibility is of order $1/c$ we may rewrite Eq. (10) in the form

$$R\ddot{R} = -\frac{3}{2}\dot{R}^2 + \frac{1}{\rho}\left(P_g - P_0 - P_a \cos\omega t - \frac{2\sigma}{R} - 4\mu\frac{\dot{R}}{R}\right) + O(1/c), \tag{18}$$

substitution of which in Eq. (17) yields, up to order $1/c$,

$$\begin{aligned}\frac{\dddot{V}}{4\pi c} &= \frac{1}{2c}\dot{R}^3 + \frac{1}{c}R\dot{R}\ddot{R} \\ &\quad + \frac{1}{\rho c}\frac{d}{dt}\left[R\left(P_g - P_0 - P_a\cos\omega t - \frac{2\sigma}{R} - 4\mu\frac{\dot{R}}{R}\right)\right] .\end{aligned} \tag{19}$$

Adding this approximation of $\dddot{V}/4\pi c$ to the right-hand side of Eq. (10) and rearranging yields

$$\begin{aligned}\left(1 - \frac{\dot{R}}{c}\right)R\ddot{R} + \frac{3}{2}\left(1 - \frac{\dot{R}}{3c}\right)\dot{R}^2 &= \frac{1}{\rho}\left(1 + \frac{\dot{R}}{c} + \frac{R}{c}\frac{d}{dt}\right) \\ &\quad \times \left(P_g - P_0 - P_a\cos\omega t - \frac{2\sigma}{R} - 4\mu\frac{\dot{R}}{R}\right) .\end{aligned} \tag{20}$$

7

This formulation is equivalent to Keller's equation [13] at order $1/c$ [like Eq. (20), Keller's equation is only accurate to order $1/c$]. One reason for our use of Eq. (20) is its derivation from the compressibility term $\ddot{V}/4\pi c$, the physical origin of which is easy to understand. [12] Another reason is that there is a slight computational advantage to coding Eq. (20) for acoustic pressures $P_a(t)$ that are more complicated than the simple sinusoidal excitation $P_a \cos \omega t$ considered in the present work, e.g., sonar signals or lithotripsy shock waves. The Keller formulation requires evaluation of a time shifted pressure $P_a[t + R(t)/c]$ rather than a pressure and its derivative at the instantaneous time t.

B.   Temperature dependence of Henry's law

Bubble oscillation generates a finite temperature gradient in the surrounding liquid that is proportional to the excitation level and the temperature of the surrounding water. [14] The effect of this gradient on the bubble dynamics was shown to be negligible for the case studied in Ref. [14], but gas solubility is also temperature dependent, and has not previously been accounted for in rectified diffusion studies.

Henry's law for our case is given by Eq. (3), where H_D depends on temperature. In Ref. [15] there are the tables for Henry's constants and their temperature dependencies. Our definition of H_D corresponds to $(\mathcal{N} k_H)^{-1}$ in Ref. [15], where $\mathcal{N}$ is the Avogadro constant and k_H is the concentration of a species in the aqueous phase divided by the partial pressure of that species in the gas phase. Therefore $d = k_B T_0/H_D$ corresponds to k_H^{cc} for $T = T_0$ in Ref. [15], where k_H^{cc} is the dimensionless ratio of the aqueous-phase concentration of a species to its gas-phase concentration .

According to Ref. [15], the measurements fall in the ranges $0.0149 < k_H^{cc} < 0.0159$ for nitrogen and $0.0294 < k_H^{cc} < 0.0318$ for oxygen. Using mean values of the reported ranges and approximating air as 80% nitrogen and 20% oxygen we take $k_H^{cc} = 0.019$, which yields the value $d(T_0) = 0.02$ that was used in our calculations. The temperature dependence according to Ref. [15] is

$$d(T) = d(T_0) \exp \left[\alpha_H \left(\frac{1}{T} - \frac{1}{T_0} \right) \right] , \tag{21}$$

where $\alpha_H = 1300\,\mathrm{K}$ for nitrogen.

C. Heat conduction in the gas

A polytropic equation of state for the gas inside the bubble was used in Ref. [1], which is common practice because of its ease of implementation. This approach has been shown to be inadequate for large amplitude motion. [14, 16] Further, the model in Ref. [14] describes heat conduction in the absence of mass flux. In this section, we develop a model for heat conduction in the gas that accurately describes bubble growth by rectified diffusion under high amplitude acoustic excitation, and which explicitly accounts for mass flux across the bubble wall.

The thermometric conductivity χ_g of the gas is

$$\chi_g = \nu_g/\text{Pr}.\tag{22}$$

For air, $\nu_g = 0.15$ cm^2/s is the dynamic viscosity coefficient and $\text{Pr} = 0.733$ is the Prandtl number, and therefore $\chi_g \simeq 2.04 \times 10^{-5}$ m^2/s. The characteristic length scale for the thermal conductivity is

$$L_g = \sqrt{\chi_g/2\omega}.\tag{23}$$

For $\omega/2\pi = 100$ Hz we have $L_g = 127\,\mu$m, which means that for $R_0 \leq 100\,\mu$m we can ignore the fact that the gas temperature is not uniform inside the bubble. For $\omega/2\pi = 10$ kHz we have $L_g = 12.7\,\mu$m and $R_0 \geq 10\,\mu$m, and it is necessary to take into account the finite value of L_g. The effect of this inhomogeneity is that the equation of state for the gas is close to adiabatic and oscillations of the bubble radius are reduced. In this case rectified diffusion of the gas dissolved in the liquid is also less.

To estimate the effect of a nonuniform temperature distribution we must solve the equation for heat conduction in the gas. An equation such as Eq. (14) cannot be used because it applies only to incompressible liquids, and compressibility of the gas must be taken into account. However, for our problem the full equations of gas dynamics are unnecessary because bubble size is small compared to a wavelength, permitting the simplification whereby the gas pressure P_g may be assumed uniform inside the bubble.

To construct the finite difference scheme for this problem it is convenient to transform the radial coordinate r inside the bubble, which occupies the variable domain $0 \leq r \leq R$, to a normalized spatial coordinate ζ in the fixed domain $0 \leq \zeta \leq 1$. First the heat diffusion equation is written in coordinates that are similar to Lagrangian coordinates but permit

9

bubble growth and variation in the mass of the gas. We thus introduce the variable $m(r,t)$, which is the mass of gas inside a sphere of radius r. Introduction of this variable permits us to ignore the convection term in the heat conduction equation. The equation for the gas temperature T_g thus becomes

$$c_p \rho_g \frac{\partial T_g(m,t)}{\partial t} = \frac{1}{r^2}\frac{\partial}{\partial r}\left(\kappa_g r^2 \frac{\partial T_g}{\partial r}\right), \tag{24}$$

where c_p is the specific heat and ρ_g is the density of the gas. The thermal conductivity κ_g of the gas depends on temperature but not on pressure, and according to the kinetic theory of gases it can be taken proportional to the square root of the gas temperature,

$$\kappa_g = \kappa_{g0}\sqrt{T_g/T_{g0}}, \tag{25}$$

where κ_{g0} is the thermal conductivity at the reference temperature T_{g0}.

Introducing the reference thermometric conductivity for a gas with reference density ρ_{g0},

$$\chi_{g0} = \frac{\kappa_{g0}}{c_v \rho_{g0}}, \tag{26}$$

we may rewrite Eq. (24) as follows:

$$\frac{\partial T_g(m,t)}{\partial t} = \chi_{g0}\frac{\rho_{g0}}{\rho_g}\frac{1}{r^2}\frac{\partial}{\partial r}\left(\sqrt{\frac{T_g}{T_{g0}}}r^2\frac{\partial T_g}{\partial r}\right) \tag{27}$$

$$= \chi_{g0}\frac{\rho_{g0}}{\rho_g}\frac{\partial}{\partial(r^3/3)}\left[\sqrt{\frac{T_g}{T_{g0}}}r^4\frac{\partial T_g}{\partial(r^3/3)}\right] \tag{28}$$

$$= (4\pi)^2 \chi_{g0}\rho_{g0}^2 \frac{P_g}{P_{g0}}\frac{\partial}{\partial m}\left[\sqrt{\frac{T_{g0}}{T_g}}r^4\frac{\partial T_g}{\partial m}\right], \tag{29}$$

where the final form results from noting that

$$d[(4/3)\pi r^3] = dm/\rho_g. \tag{30}$$

The maximum value of m is $m_0(t) = MN(t)$, which is the total mass of gas in the bubble, and where M is mass per molecule and N is the number of molecules. Since this quantity changes with time it is convenient to introduce the relative mass $\zeta = m/m_0 \in (0,1)$. In terms of ζ Eq. (29) takes the form

$$\frac{\partial T_g(\zeta,t)}{\partial t} - \frac{\zeta}{N}\frac{\partial T_g}{\partial \zeta}\frac{\partial N}{\partial t} = \left(\frac{4\pi}{NM}\right)^2 \chi_{g0}\rho_{g0}^2 \frac{P_g}{P_{g0}}$$
$$\times \frac{\partial}{\partial \zeta}\left[\sqrt{\frac{T_{g0}}{T_g}}r^4\frac{\partial T_g}{\partial \zeta}\right]. \tag{31}$$

10

We can calculate r from Eq. (30):

$$r^3 = \frac{3NM}{4\pi} \int_0^\zeta \frac{d\zeta'}{\rho_g} = \frac{3NM}{4\pi\rho_{g0}} \frac{P_{g0}}{P_g} \int_0^\zeta \frac{T_g}{T_{g0}} d\zeta'. \tag{32}$$

After substituting $r^4 = (r^3)^{4/3}$ in Eq. (31) we have

$$\frac{\partial T_g(\zeta,t)}{\partial t} - \frac{\zeta}{N} \frac{\partial T_g}{\partial \zeta} \frac{\partial N}{\partial t} = \left(\frac{36\pi}{NM}\right)^{2/3} \chi_{g0} \rho_{g0}^{2/3} \left(\frac{P_{g0}}{P_g}\right)^{1/3}$$
$$\times \frac{\partial}{\partial \zeta} \left[\sqrt{\frac{T_{g0}}{T_g}} s_T^{4/3} \frac{\partial T_g}{\partial \zeta} \right], \tag{33}$$

where

$$s_T(\zeta,t) = \int_0^\zeta \frac{T_g}{T_{g0}} d\zeta'. \tag{34}$$

A semi-implicit finite-difference scheme with a homogeneous grid on the interval $\zeta \in (0,1)$ was developed to solve Eq. (33) numerically. Equation (32) permits calculation of the gas pressure P_g for any given bubble radius $R = r|_{\zeta=1}$ and gas temperature T_g.

D.   Model implementation

A computer code was written to calculate bubble growth in supersaturated liquid in the presence of a sound field via solution of a subset of equations presented in the previous sections. Gas diffusion in the liquid is described by Eq. (14), bubble dynamics by Eq. (20), and thermal conductivity of the gas in the bubble by Eq. (33). To account for heat conduction in the liquid surrounding the growing bubble an equation of the same type as Eq. (9) is solved. The time step Δt for the calculations was taken to be of order 10^{-7} s. Every time step consists of four substeps: (i) a substep for the ordinary differential equation for bubble radius and gas mass, Eqs. (20) and (11); (ii) a substep for the adiabatic expansion of the gas to achieve a new bubble radius; (iii) a substep for gas diffusion, Eq. (14); (iv) a substep for gas thermal conductivity, Eq. (31). At the end of the fourth substep the gas pressure was calculated using Eq. (32) as follows:

$$\frac{P_g}{P_{g0}} = \frac{3NM}{4\pi\rho_{g0}R^3} \int_0^1 \frac{T_g}{T_{g0}} d\zeta = \frac{3NM}{4\pi\rho_{g0}R^3} s_T|_{\zeta=1}. \tag{35}$$

Substeps (ii) and (iv) combined describe the gas thermodynamics in exactly the same way as Prosperetti et al. [14] It may be noted that their Eq. (12) depends on c_p whereas our
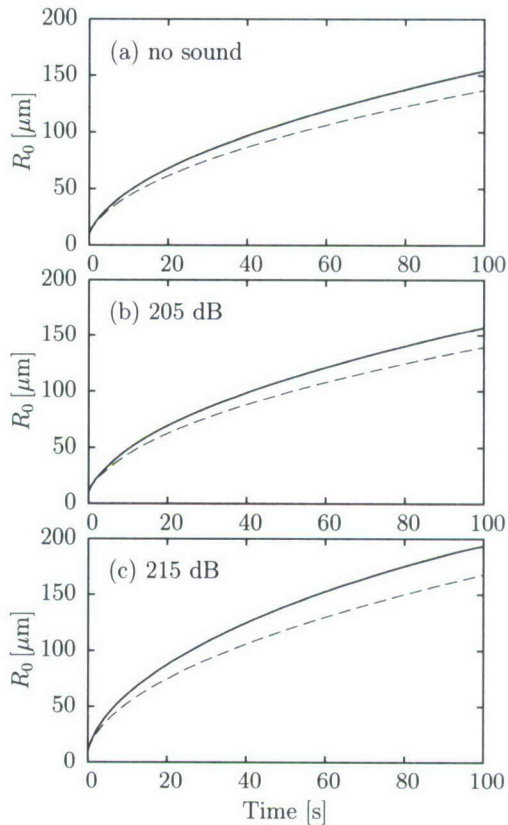
11

FIG. 1: Dependence of the equilibrium bubble radius R_0 on time for gas concentration $C_\infty/C_0 = 3$ (a) in the absence of acoustic excitation and for sound pressure levels of (b) 205 dB and (c) 215 dB (re 1 μPa) at 100 Hz. Solid lines are results obtained from the present numerical model. Dashed lines are the solutions of Eq. 8, which is Fyrillas and Szeri's model. [8]

Eq. (31), with χ_{g0} defined in Eq. (26), depends on c_v. However, when our Eq. (31) [substep (iv)] is combined with the adiabatic gas law [substep (ii)], which depends on the ratio c_p/c_v, the net result is a calculation that depends only on c_p, as in Ref. [14].

IV. RESULTS

The numerical calculations described in Section III D were performed for an air bubble in water at 300% supersaturation, which corresponds to $C_\infty/C_0 = 3$. Results are presented in Fig. 1 for (a) static diffusion in the absence of acoustic excitation, and for sound pressure levels of (b) 205 dB and (c) 215 dB (re 1 μPa) at 100 Hz. In each case the initial bubble radius was 10 μm. The physical parameters used in the calculations were those for air bubbles in

water at 20 °C: $d = 0.02$, $\rho = 10^3 \, \text{kg/m}^3$, $D = 2.4 \times 10^{-9} \, \text{m}^2/\text{s}$, $\chi_g = 2 \times 10^{-5} \, \text{m}^2/\text{s}$, $\sigma = 0.072 \, \text{N/m}$, $\mu = 0.001 \, \text{kg/ms}$, $c_p/c_v = 1.4$, and $P_0 = 10^5 \, \text{Pa}$. The number of samples in the dimensionless coordinate ξ was $n_d = 1000$, the number of samples for calculations of heat conduction in the gas was $n_g = 300$, and the number of time steps per acoustic period was $n_m = 2 \times 10^4$. In each case, results of these numerical calculations, shown with solid lines, are compared with predictions based on Eq. (8) and shown with dashed lines. In the last case, Fig. 1(c), thermal conductivity of the gas in the bubble was taken into account in the same manner as by Crum and Mao. [1] Periodic oscillations of the bubble were calculated using a standard shooting method, with the initial conditions for the bubble radius and its derivative repeated for one period of the external acoustic pressure.

It is clear from Fig. 1 that, at the high level of supersaturation used here, the contribution to bubble growth from rectified diffusion at sound pressure levels of 205 dB and below is negligible in comparison with the contribution from static diffusion. It is also seen that accounting for the finite rate of bubble growth in the present model yields a moderate amount of diffusion enhancement. For static diffusion alone [Fig. 1(a)] the present model predicts about 8% more growth than Eq. (8), while at the highest excitation level [Fig. 1(c)] the present model predicts about 18% more growth than Eq. (8).

The same calculations were repeated for different parameters, including different frequencies, bubble sizes and the treatment of the gas concentration at infinity. Calculations for 1000 Hz yield approximately the same results but take much longer because the time step must be reduced by one order of magnitude. Likewise, when the initial bubble size is varied, there is little effect on the growth, as long as the excitation is well below the bubble resonance frequency. When the supersaturation of the water far away from the bubble is held constant, the bubble radius grows monotonically. In reality the gas concentration in the surrounding liquid approaches exponentially the equilibrium concentration $C_0 = P_0/H_D$ corresponding to the external pressure P_0. We can take into account the variation of the concentration due to this relaxation process by, according to Eq. (1), adding the term $-(C - C_0)/t_w$ to the right-hand sides of Eqs. (9) and (15). In this case the gas concentration far away from the bubble will decrease exponentially with time constant t_w, and for durations of order several times t_w the concentration far away from the bubble is nearly at its equilibrium value, and bubble growth is practically stopped. For illustration, shown by solids lines in Fig. 2 are the results of a calculation with $t_h = 360 \, \text{s}$ for static diffusion and for a sound pressure level of
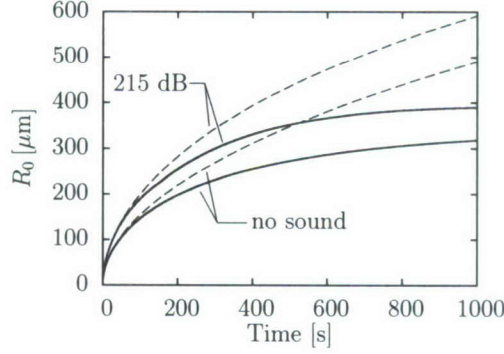
13

FIG. 2: Dependence of the equilibrium bubble radius R_0 on time with and without sound for washout half times of $t_h = 360$ s (solid lines) and $t_h = \infty$ (dashed lines).

215 dB, but otherwise for the same parameters as were used for Fig. 1. This washout time corresponds to muscle tissue for both dolphins [3] and humans [17]. Shown for comparison on the same graph are dashed lines for the same parameters but with $t_w = \infty$, i.e., for constant $C_\infty/C_0 = 3$.

To investigate the temperature dependence of Henry's constant and thermal conductivity of the gas we included Eqs. (21) and (25) in the numerical calculations. It was found that the influence of the temperature dependence of Henry's constant is negligible when the surrounding liquid is at 20 °C. At this equilibrium temperature, changes in the temperature of the liquid near the bubble are very small because of the high thermal conductivity of the liquid in comparison with the thermal conductivity of the gas. There was less than a 0.1% change in bubble growth when Eq. (21) was used. This effect could become more important if the surrounding liquid is at an elevated temperature. For example, the case studied in Ref. [14], which was for an air bubble of radius 0.1 cm at resonance, in water with a temperature of 100 °C, the temperature gradient is more than thirty times larger than the gradient at 20 °C. [14] The effect of radiation losses was studied by substituting Eq. (10) for Eq. (20) in the numerical calculations. For the relatively low acoustic frequencies studied here, 100 Hz–1000 Hz, the influence of radiation losses on bubble growth is also negligible.

For all the cases discussed above, the results for bubble growth are higher than what are obtained using models such as Eqs. (7) and (8). Kamath and Prosperetti [18] also observed an increased bubble growth rate using direct numerical solution of the diffusion equation, but they considered only low supersaturation levels near the threshold of bubble growth and did not consider the high supersaturation level used here. A difference between our results

14

and those obtained with models of the type given by Eqs. (7) and (8) is that the latter do not take into account the influence of systematic bubble growth on gas diffusion. The gradient of the dissolved gas concentration $\partial C / \partial r$, and the mass flow of gas into the bubble dm_g/dt according to either Eq. (5) or (7), are estimated for a given equilibrium bubble radius. In reality this gradient and mass flow depend on the growth rate of the equilibrium bubble radius. It can be shown that the correction introduced by the bubble growth rate becomes significant when the characteristic time for bubble growth $t_R = R^2/[Dd(C_\infty/C_0)-1]$ approaches the characteristic time of gas diffusion near the bubble, $t_D = R^2/D$. The ratio $t_D/t_R = d(C_\infty/C_0 - 1)$ does not depend on D and is of order 0.1 for high levels of the supersaturation $C_\infty/C_0 - 1$. This in turn means that the growth rate correction may be of order 10% or more. This approximation is indeed borne out, as nearly the same difference in bubble growth appears in Fig. 1 between the predictions of the present model and Eq. (8).

In the remaining sections, bubble growth will be investigated for a variety of acoustic excitations that are similar to sonar signals. The maximum sound pressure level used in these calculations is 215 dB (re 1 μPa). Note that the use of "source level" to characterize the acoustic output of a transducer does not imply that the acoustic pressure is ever actually as high as the stated source level. By definition, source level is an inferred quantity. The acoustic pressure radiated by a transducer is measured in the acoustic far-field, and then scaled back to a range of 1 m via spherical spreading. [19] The maximum sound pressure level near the source never achieves a level equal to the source level, as illustrated in Fig. 3. The solid curve was calculated using Eq. (7.4.5) of Ref. [20], which is for on-axis radiation from a piston in an infinite baffle, and shows the characteristic pattern of maxima and minima found in the near field of a transducer. The piston for this calculation is 2 m in diameter, radiating at 3 kHz with a source level of 235 dB (re 1 μPa), as illustrated by the dashed line, which is typical of the source level of mid-frequency active sonars. The maximum sound pressure level near the transducer is 212 dB.

A.   Effect of Gas Concentration for Continuous Wave Signals

The calculations that were described in Section III D, and presented as solid lines in Fig. 1 are computationally intensive. For example, the solid curves in Fig. 1 required several hours to compute on a desktop computer. In comparison, the dashed curves require only minutes
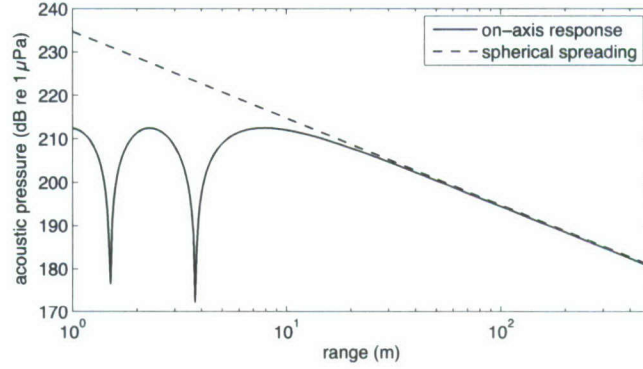
FIG. 3: The on-axis sound pressure level radiated by a piston in an infinite baffle is shown with the solid line. The dashed line indicates how the far-field acoustic pressure is scaled back to a range of 1 m via spherical spreading for the purpose of determining the source level. This transducer's source level is 235 dB (re 1 μPa), but the maximum sound pressure level actually radiated by the transducer is only 212 dB.
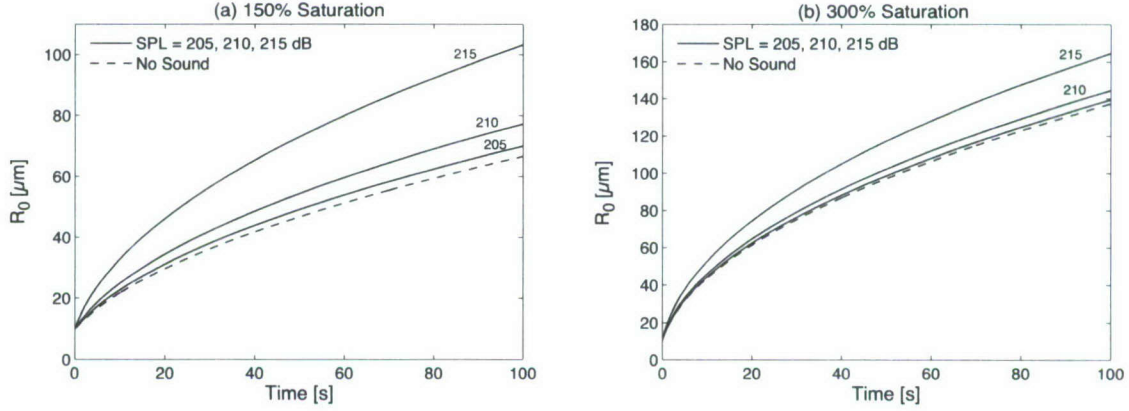

FIG. 4: The effect of gas concentration is shown through dependence of the equilibrium bubble radius R_0 on time, for CW acoustic excitation at 1 kHz and SPLs ranging from 205 dB to 215 dB (re 1 μPa), and for gas concentrations $C_\infty/C_0 = 1.5$ (a) and $C_\infty/C_0 = 3$ (b). The initial equilibrium bubble radius was 10 μm.

and they result in predictions that are only a few percent too low. In order to facilitate the study of a much larger parameter space, the remaining calculations were conducted using the method previously described for the dashed lines in Fig. 1, that is, using Eq. (8) and Eq. (36) in the Appendix. Figure 4 shows the effect of gas concentration for continuous wave (CW) signals at 1 kHz for an initial equilibrium bubble radii of 10 μm. At a gas concentration
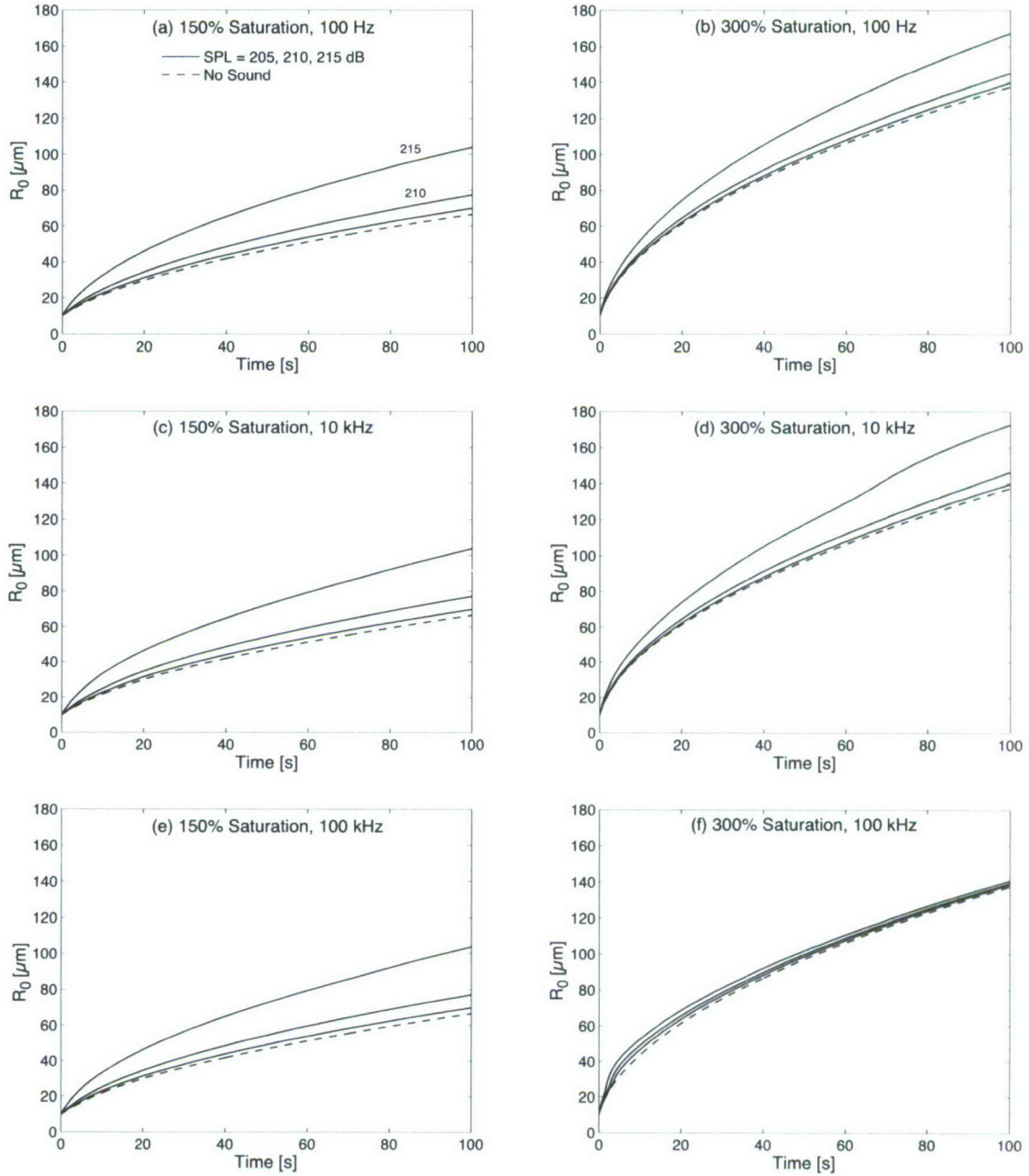
16

FIG. 5: The effect of excitation frequency is shown through dependence of the equilibrium bubble radius R_0 on time, for CW acoustic excitation at various frequencies and SPLs ranging from 205 dB to 215 dB (re 1 μPa). Gas concentration $C_\infty/C_0 = 1.5$ is shown in (a), (c) and (e), and $C_\infty/C_0 = 3$ in (b), (d) and (f). In all cases, increasing SPL monotonically shifts the growth curves to higher values, as labeled in (a). The legend and the dB values are the same for the remaining plots. The initial equilibrium bubble radius was 10 μm for all cases.

of 150% supersaturation, there is little significant bubble growth beyond that provided by static diffusion alone (no sound), at acoustic excitation levels below 210 dB. At higher acoustic excitation levels, bubble growth is enhanced by acoustic excitation. For example, after 100 seconds at 215 dB, the acoustically driven bubble is about 60% larger than the bubble with no sound. At an increased gas concentration of 300%, the acoustic excitation has a smaller effect. There is only a 20% increase in bubble growth under an acoustic excitation of 215 dB, as compared to static diffusion alone (no sound).

B.   Effect of Excitation Frequency for Continuous Wave Signals

The calculations presented in the previous section (Section IV A) were repeated for different frequencies and the results are shown in Fig. 5. In all cases, the acoustic excitation was CW, but the frequencies 100 Hz, 10 kHz and 100 kHz were used. The left column of Fig. 5 shows gas concentrations of 150% and the right column shows 300%. The drive frequency has little effect at 150% supersaturation. The bubble growth is nearly the same for all three drive frequencies, across all three drive amplitudes. For higher gas concentration, increasing frequency initially causes a slight increase in bubble growth, as seen when comparing Fig. 5(b) and (d) at times greater than about 60 seconds. As the frequency increases, it appears that rectified diffusion is eliminated. There is no significant difference between bubble growth by static diffusion (no sound) and the three cases with acoustic excitation. Even at the highest amplitude, 215 dB, bubble growth is dominated by static diffusion.

The effect of excitation frequency is demonstrated in another way in Fig. 6. The equilibrium bubble radius $R_0(t = 100)$ after 100 seconds of acoustic excitation was calculated for a variety of drive amplitudes and for five excitation frequencies: 10^2, 10^3, 10^4, 3×10^4 and 10^5 Hz. At a gas concentration of 150% supersaturation, the curves for all five drive amplitudes are flat below 10^4 Hz, which indicates that the excitation frequency has a negligible effect on bubble growth when the drive frequency is below bubble resonance. The bubble growth increases as the drive frequency approaches bubble resonance, and then decreases above resonance. For example in Fig. 6(a) at a drive amplitude of 210 dB, the curve is flat through $f = 10$ kHz, which coincides with a bubble radius of 80 μm. At this size, the resonance frequency is about 40 kHz, and hence the bubble is being driven below resonance. At $f = 30$ kHz, one finds a bubble size of 85 μm, which has a resonance frequency of about
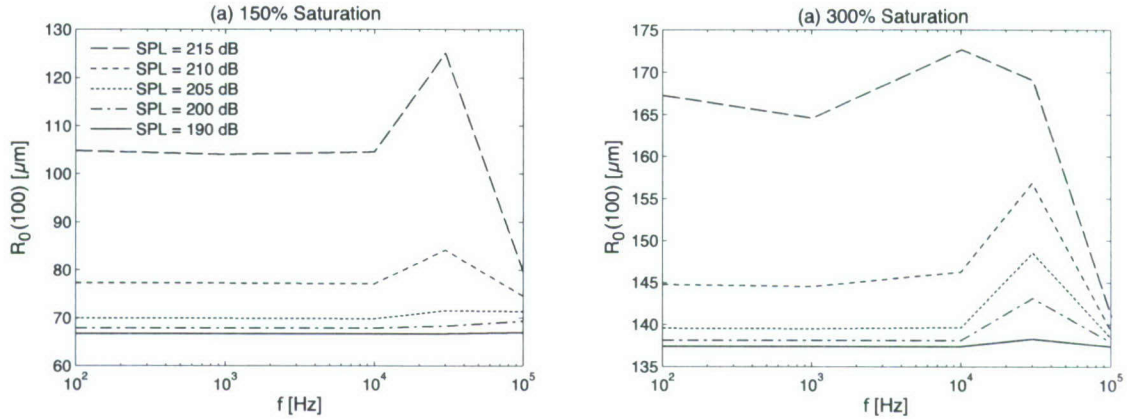
FIG. 6: The equilibrium bubble radius $R_0(100)$ after $t = 100$ seconds of excitation is plotted as a function of excitation frequency, for various drive levels and two gas concentrations.

37 kHz, hence the drive frequency is approaching resonance and the bubble growth has increased over that at subresonance drive frequencies. Well above the resonance frequency, the bubble wall motion is significantly reduced, which leads to lower bubble growth rates. A similar behavior is seen for a gas concentration of 300% supersaturation. Frequency has little effect on rectified diffusion unless the acoustic excitation frequency becomes similar to the bubble resonance frequency.

C.   Effect of Duty Cycle and Repetition Rate for Gated Sinusoidal Signals

Because continuous wave signals continuously deliver energy to an oscillating bubble, they will lead to the maximum bubble growth by rectified diffusion. Underwater acoustic communication systems typically use CW signals while transmitting data, but echolocation sonar systems do not. Gated signals are used instead. In this section, we repeat the calculations that were performed in Section IV A but for gated sinusoidal signals. Such a signal is illustrated in Fig. 7 with period T_{rep} and duty cycle $DC = \tau/T_{rep}$. Bubble growth was calculated as in Section IV A, with $T_{rep} = 10$ seconds, for various duty cycles DC and two gas concentrations. The frequency of the sinusoid was 1 kHz and the excitation level was 215 dB (re 1 μPa). Initial equilibrium bubble radius was 10 μm. The results are shown in Fig. 8. As expected, the growth due to low duty cycles is not significantly higher than growth due to static diffusion alone (no sound) for 150% supersaturation, but as duty cycle increases toward 100%, growth increases. At 300% gas concentration, there is even less significant
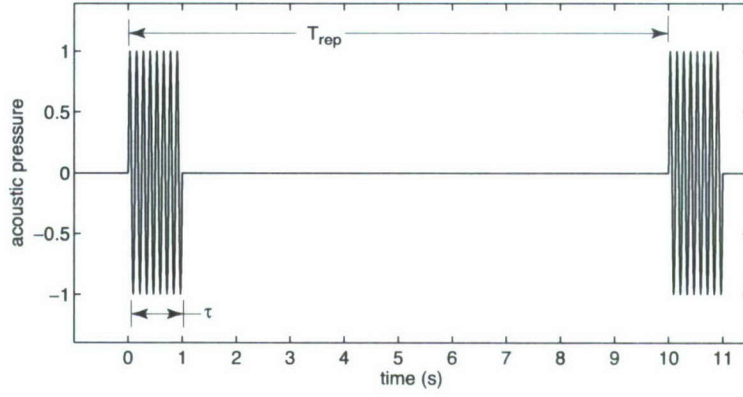
19

FIG. 7: A gated sinusoidal signal is shown with period T_{rep} and duty cycle $DC = \tau/T_{\text{rep}}$.
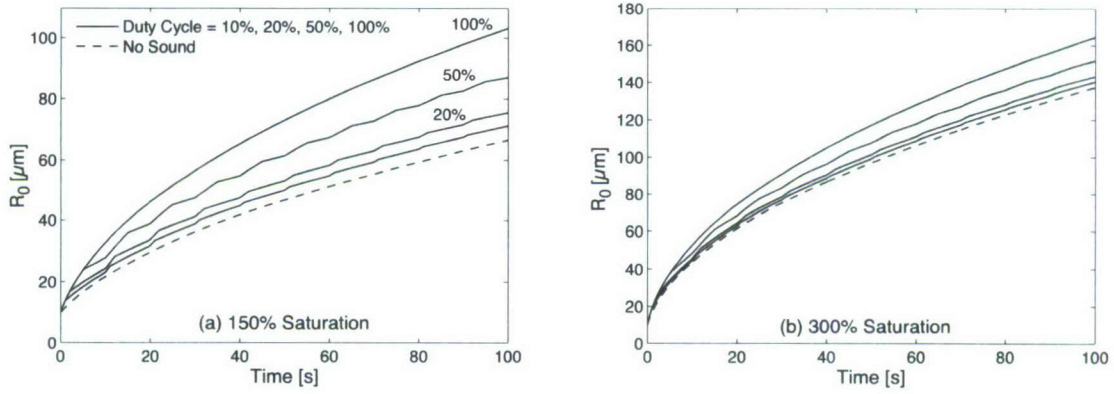

FIG. 8: The effect of duty cycle is shown through dependence of the equilibrium bubble radius R_0 on time, for gated sinusoidal acoustic excitation with a carrier frequency of 1 kHz and an SPL of 215 dB re 1 μPa (during the active part of the period), and for gas concentrations $C_\infty/C_0 = 1.5$ (a) and $C_\infty/C_0 = 3$ (b). The initial equilibrium bubble radius was 10 μm.

growth enhancement due to rectified diffusion. For the typical sonar duty cycles of 10% to 20%, the bubble growth due to rectified diffusion is less than 4% greater than growth due to static diffusion alone (no sound).

The bubble growth due to a gated signal was found to be the same as bubble growth due to a CW signal of lower amplitude. The equivalent CW SPL is shown in Fig. 9 for gated signals of various duty cycles DC and a peak pressure level of 215 dB (re 1 μPa). The other parameters are the same as in Fig. 8. The solid lines were determined by the relation: $216 + 10\log_{10}[DC/100\%]$ dB. When considered over multiple pings, the
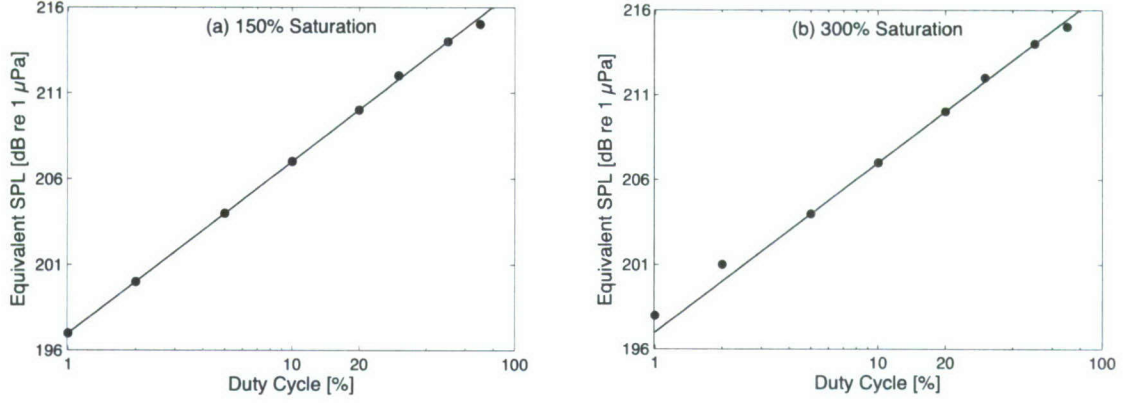
20

FIG. 9: The equivalent CW SPL is shown, for gated sinusoidal acoustic excitation with a carrier frequency of 1 kHz and a peak SPL of 215 dB (re 1 μPa), and for gas concentrations $C_\infty/C_0 = 1.5$ (a) and $C_\infty/C_0 = 3$ (b). The initial equilibrium bubble radii were 10 μm.
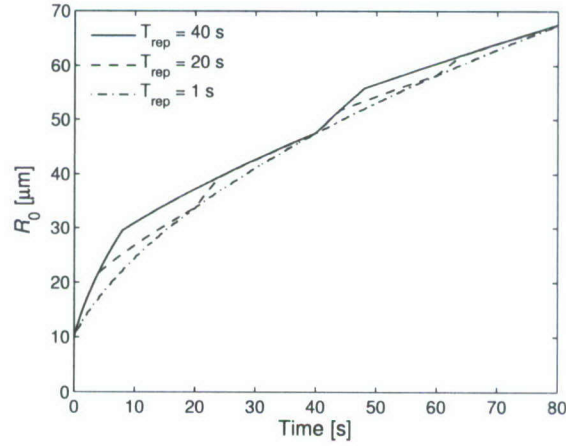

FIG. 10: The effect of repetition rate T_{rep} is shown for gated sinusoidal acoustic excitation with a carrier frequency of 1 kHz, a peak SPL of 215 dB (re 1 μPa), a duty cycle of 20%, and a gas concentration $C_\infty/C_0 = 1.5$. The initial equilibrium bubble radii were 10 μm. When different sonar periods end at the same time, $R_0(t)$ is equal for each case, such as at 40 and 80 seconds.

sonar repetition rate T_{rep} was found to have a minor effect on bubble growth, as long as the parameters of duty cycle and SPL were the same. This is illustrated in Fig. 10 for a sinusoidal frequency of 1 kHz.
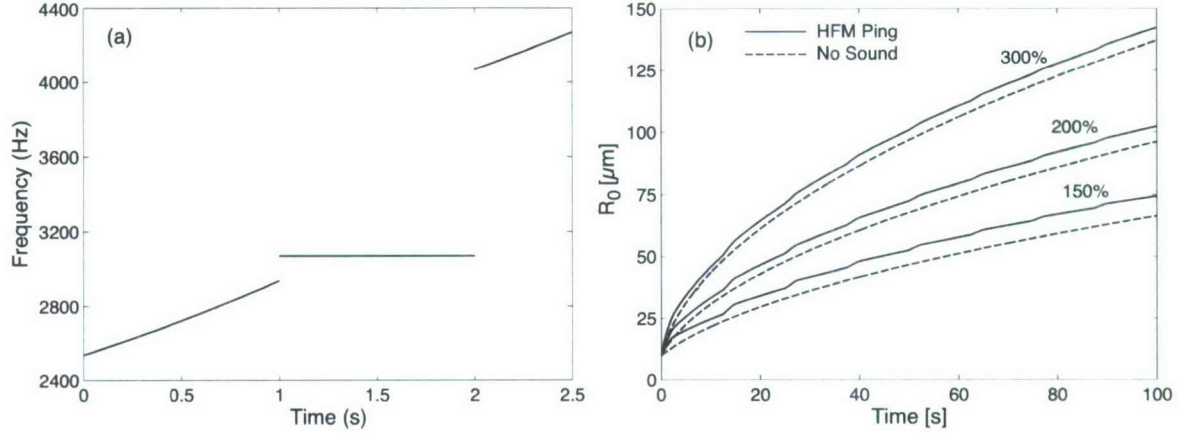
FIG. 11: The frequency content of a typical hyperbolic frequency modulated (HFM) sonar ping is shown in (a). Bubble growth (b) due to HFM pings at 20% duty cycle and three gas concentrations, compared to static diffusion (no sound). The repetition rate was $T_{rep} = 12.5$ seconds and the peak SPL of signal was 215 dB re 1 μPa.

D. Bubble Growth Due to Hyperbolic Frequency Modulated Signals

Hyperbolic frequency modulated (HFM) signals are often used in radar and sonar systems. The frequency content of such a signal is shown in Fig. 11(a) and a typical duty cycle is 20% with a repetition rate of $T_{rep} = 12.5$ seconds. The calculations described in Section IV A were repeated for such a signal with a peak SPL of 215 dB (re 1μPa). This excitation causes a minor increase in bubble growth as compared to bubble growth due to static diffusion alone (no sound), as shown in Fig. 11(b). For the highest gas concentration level, 300% supersaturation, the increase in bubble size due to rectified diffusion is about 5%, and for 150% supersaturation, the increase is about 12%. The initial equilibrium bubble size was 10 μm.

E. Passive Growth and Dissolution of Bubbles at Zero Depth in Muscle Tissue

Another case of interest is the long-term passive growth of bubbles at zero depth, such as might be applicable to a stranded marine mammal. At the surface, subject to atmospheric pressure, the muscle tissue gas supersaturation will decrease and eventually reach atmospheric levels. While this is occurring, the bubble will grow while the tissue is supersaturated, but once the pressure of gas in the bubble is greater than that in the tissue (due
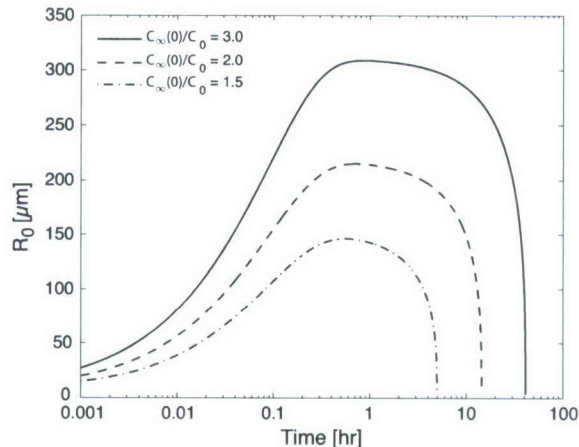
22

FIG. 12: Passive bubble growth in a stranded marine mammal.

to surface tension), the bubble is not stable and will dissolve. This is illustrated for three initial gas concentrations in Fig. 12. The washout half-time $t_h = 360$ seconds was used, which corresponds to muscle tissue of dolphins [3] and humans. [17] The maximum bubble size is reached after about 48 minutes at 300% concentration, after about 42 minutes for 200% and after about 33 minutes for 150%.

V. CONCLUSIONS

For high gas supersaturation levels in liquids, on the order of 300% as predicted in capillaries of marine mammals following a series of dives, [2] standard mathematical models of both static and rectified diffusion were found to underestimate the rate of bubble growth by 10%–20%. The discrepancy was demonstrated by comparing predictions based on existing mathematical models with direct numerical solutions of the differential equations for gas diffusion in the liquid and thermal conditions in the bubble. Underestimation of bubble growth by existing mathematical models is due to the underlying assumption that the gas concentration in the liquid is given by its value for a bubble of constant equilibrium radius. This assumption is violated when high supersaturation causes the bubble to grow too fast in relation to the time scale associated with diffusion. Rapid bubble growth results in an increased gas concentration gradient at the bubble wall, and therefore a growth rate in excess of predictions based on constant equilibrium bubble radius. We also studied the dependence of Henry's "constant" on temperature and found that it was not significantly temperature

23

dependent and can be accurately represented as a constant.

The direct numerical computations that account for this (and that were presented in Fig. 1) are computationally intensive. To explore a wider range of the parameter space, such as the effect of frequency, and the effect of using pulsed signals and chirps, additional calculations were performed using the model of Fyrillas and Szeri, [8] which is the next most accurate model and less computationally intensive. The results presented here, for the idealized conditions of a preexisting single spherical bubble in a pure infinite fluid, absent of any surfactants or stabilization mechanisms, indicate that acoustic excitation typical of sonar systems results in minor enhancement of bubble growth over that of static diffusion alone (no sound). For the highest level of gas concentration studied here, 300% supersaturation, and for a realistic sonar ping with a peak SPL of 215 dB (re 1 μPa) at the bubble and a duty cycle of 20%, there is only about a 5% increase in bubble growth due to rectified diffusion. Note that at 300% saturation, the results obtained with the model of Fyrillas and Szeri [8] underestimate the growth by 10%–20%. It was also shown that frequency plays a minor role in bubble growth, unless the excitation frequency coincides with the resonance frequency for the bubble at some time in its growth history. Gated sinusoidal signals with less than a 100% duty cycle cause bubble growth that can be simply related to a lower-amplitude CW signal. There are no additional effects due to excitation by an HFM chirp, as compared a gated sinusoid. Any gated signal will produce less bubble growth than its CW counterpart. Finally, for static diffusion at atmospheric pressure, under conditions that mimic those potentially experienced by a stranded marine mammal, bubbles were found to grow passively to their maximum size in about 40–50 minutes, followed by a reduction in size and eventual dissolution in 5 to 40 hours, depending on initial gas concentration.

In separate but related studies, the authors and their collaborators investigated the effect of tissue shear elasticity on the dynamics of bubbles, [21, 22] confinement of bubbles by plates and tubes, [23, 24] and coalescence of bubbles. [25–27] For bubbles in elastic tissue, the increased effective external pressure due to tissue shear elasticity inhibits bubble growth as compared to a bubble in a liquid. For bubbles in tubes, any confinement by walls inhibits flow and bubble oscillation, hence confined spaces also inhibit bubble growth, compared to free bubbles. Under high amplitude excitation, such as that due to a lithotripter shock wave (peak pressures of order 10 MPa), micron-size bubbles can grow dynamically and coalesce into significantly larger bubbles. It is also possible that neighboring micron size bubbles

24

could grow by rectified diffusion and coalesce into larger bubbles. Knowledge of the density and distribution of bubble nucleation sites would be required to further investigate this effect.

Finally, we reiterate that our calculations were performed for the idealized system of a preexisting single bubble in a pure liquid of infinite extent. The significant and potentially complex issue of bubble nucleation was not addressed. [1, 4] A sound source is a necessary, but insufficient condition for bubble growth. Supersaturated fluids or tissues and stabilized bubble nuclei must exist. A sound source can destabilize bubbles, which then grow primarily by static diffusion. Further, *in vivo* bubble dynamics is a complicated process affected by many factors, such as constraints imposed by tissue, nonspherical bubble shapes, surfactants and potential bubble coalescence. Uncertainties associated with such additional factors can easily dominate the contribution due to the percentage change in growth rate predicted here in connection with rectified diffusion in an unbounded liquid.

Appendix

The form of the Rayleigh-Plesset equation used in Sections IV A through IV E is:

$$R\ddot{R} + \frac{3}{2}\dot{R}^2 = \frac{1}{\rho}\left[\left(P_0 + \frac{2\sigma}{R_0}\right)\left(\frac{R_0}{R}\right)^{3\eta} - P_0 - \frac{2\sigma}{R} \right. \tag{36}$$
$$\left. + P_a \sin\omega t - \frac{4\mu}{R}\dot{R} - \rho R_0 \frac{\omega_0^2}{\omega}\left(b_r + b_t\right)\dot{R}\right],$$

where σ is the surface tension, ω is the angular frequency of the acoustic source, and μ is the coefficient of shear viscosity. [1] The angular resonance frequency of the bubble ω_0 is

$$\omega_0^2 = \frac{1}{\rho R_0^2}\left[3\eta\left(P_0 + \frac{2\sigma}{R_0}\right) - \frac{2\sigma}{R_0}\right]. \tag{37}$$

The polytropic index η is defined by

$$\eta = \gamma\left(1 + b_t^2\right)\left[1 + \frac{3\left(\gamma - 1\right)}{X}\left(\frac{S_-}{C_-}\right)\right]^{-1}, \tag{38}$$

where

$$S_{\pm} = \sinh X \pm \sin X, \tag{39}$$

$$C_- = \cosh X - \cos X, \tag{40}$$

$$X = R_0\left(2\omega/D_1\right)^{1/2}, \tag{41}$$

and D_1 is the thermal diffusion constant of the gas. The thermal damping constant is

$$b_t = 3\left(\gamma - 1\right)\left[\frac{X S_+ - 2 C_-}{X^2 C_- + 3\left(\gamma - 1\right) X S_-}\right]. \tag{42}$$

The radiation damping constant b_r is given by

$$b_r = \frac{\rho R_0^3 \omega^3}{3\eta\left(P_0 + 2\sigma/R_0\right) c\left\{1 - 2\sigma/\left[3\eta R_0\left(P_0 + 2\sigma/R_0\right)\right]\right\}}. \tag{43}$$

[1] L. A. Crum and Y. Mao, "Acoustically enhanced bubble growth at low frequencies and its implications for human diver and marine mammal safety," J. Acoust. Soc. Am. **99**, 2898–2907 (1996).

[2] D. S. Houser, R. Howard, and S. Ridgway, "Can diving-induced tissue nitrogen supersaturation increase the chance of acoustically driven bubble growth in marine mammals?," J. Theor. Biol. **213**, 183–195 (2001).

[3] S. H. Ridgway and R. Howard, "Dolphin lung collapse and intramuscular circulation during free diving: evidence from nitrogen washout," Science **206**, 1182–1183 (1979).

[4] L. A. Crum, M. R. Bailey, J. Guan, P. R. Hilmo, S. G. Kargl, T. J. Matula, and O. A. Sapozhnikov, "Monitoring bubble growth in supersaturated blood and tissue ex vivo and the relevance to marine mammal bioeffects," Acoustics Research Letters Online **6**, 214–220 (2005).

[5] P. S. Epstein and M. S. Plesset, "On the stability of gas bubbles in liquid-gas solutions," J. Chem. Phys. **18**, 1505–1513 (1950).

[6] A. Eller, "Bubble growth by diffusion in an 11-khz sound field," J. Acoust. Soc. Am. **52**, 1447–1449 (1972).

[7] A. Eller and H. G. Flynn, "Rectified diffusion during nonlinear pulsations of cavitation bubbles," J. Acoust. Soc. Am. **37**, 493–503 (1965).

[8] M. M. Fyrillas and A. J. Szeri, "Dissolution or growth of soluble spherical oscillating bubbles," J. Fluid Mech. **277**, 381–407 (1994).

[9] A. Prosperetti and A. Lezzi, "Bubble dynamics in a compressible liquid.," J. Fluid. Mech. **168**, 457–478 (1986).

[10] A. Prosperetti, "The equation of bubble dynamics in a compressible liquid," Phys. Fluids Mech. **30**, 3626–3628 (1987).

[11] C. C. Church, "A theoretical study of cavitation generated by an extracorporeal shock wave lithotripter," J. Acoust. Soc. Am. **86**, 215–227 (1989).

[12] Yu. A. Ilinskii and E. A. Zabolotskaya, "Cooperative radiation and scattering of acoustic waves," J. Acoust. Soc. Am. **92**, 2837–2841 (1992).

[13] A. Lezzi and A. Prosperetti, "Bubble dynamics in a compressible liquid. part 2. second-order theory," J. Fluid Mech. **185**, 289–321 (1987).

[14] A. Prosperetti, L. A. Crum, and K. W. Commander, "Nonlinear bubble dynamics," J. Acoust. Soc. Am. **83**, 502–514 (1988).

[15] E. Wilhelm, R. Battino, and R. J. Wilcock, "Low-pressure solubility of gases in liquid water," Chem. Rev. **77**, 219–262 (1977).

[16] V. Kamath and A. Prosperetti, "Numerical integration methods in gas-bubble dynamics," J. Acoust. Soc. Am. **85**, 1538–1548 (1989).

[17] P. Radermacher, K. J. Falke, Y. S. Park, D. W. Ahn, S. K. Hong, J. Qvist, and W. M. Zapol, "Nitrogen tensions in brachial vein blood of Korean ama divers," J. Appl. Physiol. **73**, 2592–2595 (1992).

[18] V. Kamath and A. Prosperetti, "Mass transfer during bubble oscillations," in *Frontiers of Nonlinear Acoustics: Proceedings of the 12th Intl. Symp. on Nonlinear Acoustics*, edited by M. F. Hamilton and D. T. Blackstock (Elsevier, New York, 1990), pp. 503–508.

[19] R. J. Bobber, *Underwater Electroacoustic Measurements* (Peninsula, Los Altos, CA, 1988).

[20] L. E. Kinsler, A. R. Frey, A. B. Coppens, and J. V. Sanders, *Fundamentals of Acoustics*, 4th ed. (Wiley, New York, 2000).

[21] S. Y. Emelianov, M. F. Hamilton, Yu. A. Ilinskii, and E. A. Zabolotskaya, "Nonlinear dynamics of a gas bubble in an incompressible elastic medium," J. Acoust. Soc. Am. **115**, 581–588 (2004).

[22] E. A. Zabolotskaya, Yu. A. Ilinskii, G. D. Meegan, and M. F. Hamilton, "Modifications of the equation for gas bubble dynamics in a soft elastic medium," J. Acoust. Soc. Am. **118**, 2173–2181 (2005).

[23] J. Cui, M. F. Hamilton, P. S. Wilson, and E. A. Zabolotskaya, "Spherical bubble pulsation between parallel plates," J. Acoust. Soc. Am. **119**, 2067–2072 (2006).

[24] J. C. Atkisson, "Models for acoustically driven bubbles in channels," Ph.D. Dissertation, The University of Texas at Austin, 2008.

[25] E. A. Zabolotskaya, Yu. A. Ilinskii, G. D. Meegan, and M. F. Hamilton, "Bubble interactions

in clouds produced during shock wave lithotripsy," IEEE Ultrasonics Symposium 2004, Vol.2, 890–893 (2004).

[26] M. F. Hamilton, Yu. A. Ilinskii, G. D. Meegan, and E. A. Zabolotskaya, "Interaction of bubbles in a cluster near a rigid surface," Acoustics Research Letters Online **6**, 207–213 (2005).

[27] Yu. A. Ilinskii, M. F. Hamilton, and E. A. Zabolotskaya, "Bubble interaction dynamics in lagrangian and hamiltonian mechanics," J. Acoust. Soc. Am. **121**, 786–795 (2007).